Miner Deposita (2013) 48:585–602
DOI 10.1007/s00126-012-0448-x

ARTICLE

Re–Os molybdenite ages and zircon Hf isotopes of the Gangjiang porphyry Cu–Mo deposit in the Tibetan Orogen

Cheng-Biao Leng · Xing-Chun Zhang · Hong Zhong · Rui-Zhong Hu · Wei-De Zhou · Chao Li

Received: 28 October 2011 / Accepted: 6 November 2012 / Published online: 24 November 2012

Abstract The Miocene porphyry Cu–(Mo) deposits in the Gangdese orogenic belt in southern Tibet were formed in a post-subduction collisional setting. They are closely related to the Miocene adakite-like porphyries which were probably derived from a thickened basaltic lower crust. Furthermore, mantle components have been considered to have played a crucial role in formation of these porphyry deposits (Hou et al. Ore Geol Rev 36: 25–51, 2009; Miner Deposita doi:10.1007/s00126-012-0415-6, 2012). In this study, we present zircon Hf isotopes and molybdenite Re–Os ages on the newly discovered Gangjiang porphyry Cu–Mo deposit in southern Tibet to constrain the magma source of the intrusions and the timing of mineralization. The Gangjiang porphyry Cu–Mo deposit is located in the Nimu ore field in the central Gangdese porphyry deposits belt, southern Tibet. The copper and molybdenum mineralization occur mainly as disseminations and veins in the overlapped part of the potassic and phyllic alteration zones, and are predominantly hosted in the quartz monzonite stock and in contact with the rhyodacite porphyry stock. SIMS zircon U–Pb dating of the pre-mineral quartz monzonite stock and late intra-mineral rhyodacite porphyry yielded ages of 14.73±0.13 Ma (2σ) and 12.01±0.29 Ma (2σ), respectively. These results indicate that the magmatism could have lasted as long as about 2.7 Ma for the Gangjiang deposit. The newly obtained Re–Os model ages vary from 12.51±0.19 Ma (2σ) to 12.85±0.18 Ma (2σ) for four molybdenite samples. These Re–Os ages are roughly coincident with the rhyodacite porphyry U–Pb zircon age, and indicate a relatively short-lived episode of ore deposition (ca. 0.3 Ma). In situ Hf isotopic analyses on zircons by using LA-MC-ICP-MS indicate that the $\varepsilon_{Hf}(t)$ values of zircons from a quartz monzonite sample vary from +2.25 to +4.57 with an average of +3.33, while zircons from a rhyodacite porphyry sample vary from +5.53 to +7.81 with an average of +6.64. The Hf data indicate that mantle components could be partly involved in the deposit formation, and that mantle contributions might have increased over time from ca. 14.7 to 12.0 Ma. Combined with previous works, it is proposed that the Gangjiang deposit could have resulted from the convective thinning of the lithospheric root, and the input of upper mantle components into the magma could have played a key role in the formation of the porphyry deposits in the Miocene Gangdese porphyry copper belt in the Tibetan Orogen.

Keywords Hf isotopes · Re–Os dating · Gangjiang porphyry Cu–Mo deposit · Gangdese · Tibet

Editorial handling: F. Barra

C.-B. Leng · X.-C. Zhang (✉) · H. Zhong · R.-Z. Hu
State Key Laboratory of Ore Deposit Geochemistry, Institute of Geochemistry, Chinese Academy of Sciences, Guiyang, Guizhou 550002, China
e-mail: zhangxingchun@vip.gyig.ac.cn

C.-B. Leng
e-mail: lcb8207@163.com

W.-D. Zhou
Sichuan Institute of Metallurgical Geology and Exploration, Chengdu 610051, China

C. Li
National Research Center of Geoanalysis, Beijng 100037, China

Introduction

Porphyry deposits are currently the world's primary source of Cu and Mo and also an important source of Au (Richards 2003), making them valuable exploration targets. They occur mainly in continental margins or island arc settings (Sillitoe 1972, 2010; Corbett and Leach 1998; Cooke et al.

2005), and are intimately associated with subduction-related magmas (Richards 2003, 2011). In arc settings, hot, hydrous, relatively oxidized, sulfur-rich mafic magmas derived from the metasomatized mantle wedge undergo MASH processes (crustal melting, assimilation, magmatic storage, and homogenization) at the base of the overlying crust. These processes yield evolved, volatile-rich, metalliferous, hybrid intermediate melts, which is widely accepted as a key requirement for generating porphyry Cu deposits in arc settings (Richards 2003, 2011). However, it has recently been recognized that the porphyry deposits can also form in post-subduction collisional settings (Richards 2009), such as the Gangdese porphyry copper belt (GPCB) in southern Tibet, China (e.g., Hou et al. 2009, and references therein). Porphyry Cu–(Mo) deposits in this belt are genetically related to Miocene adakite-like porphyries (Chung et al. 2003; Hou et al. 2004, 2009; Gao et al. 2007; Guo et al. 2007). However, both the genesis of the Cu-bearing adakite-like magmas and their genetic link with porphyry Cu deposits in the GPCB remains highly controversial (Hou et al. 2012). Chung et al. (2003) and Hou et al. (2004) proposed that these adakite-like porphyries were derived from newly formed thickened basaltic lower crust, which was further confirmed by Guo et al. (2007) and Li et al. (2011). However, as adakite-like rocks derived from lower continental crust contain significantly lower Cu contents than adakites produced by oceanic slab melting, as well as normal arc andesites (cf. Sun et al. 2011), Hou et al. (2009, 2012) proposed that the interaction of mantle components with juvenile lower crust is a key process for the formation of the Miocene porphyry deposits. Recently, Li et al. (2011) proposed that this newly formed lower crust derived from partial melting of the mantle wedge would be enriched in F, Cl, H_2O, and Cu, important for formation of porphyry deposits in the GPCB. However, Qu et al. (2004, 2007) argued that these adakite-like porphyries originated from partial melting of subducted oceanic crust.

The Gangjiang Cu–Mo deposit is a recently discovered porphyry deposit in the GPCB, which was found in 2006–2008 by Lhasa Tianli Mining Co. Ltd., a joint venture between Central China Goldfields Plc. (GGG) and the Sichuan Institute of Metallurgical Geology and Exploration. Currently, resources are estimated at 1.30 million tonnes of contained Cu and 0.15 million tonnes of contained Mo with an average grade of 0.25–0.45 % Cu and 0.02–0.04 % Mo (Zhang and Zhou 2006, unpublished exploration report). In comparison with other porphyry deposits in the GPCB (such as Qulong, Chongjiang, and Tinggong), which have been studied by various researchers (Hou et al. 2004; Zheng et al. 2004; Qu et al. 2007, 2009; Li et al. 2007; Yang et al. 2009), only a few studies have been undertaken on the Gangjiang deposit (Zhang et al. 2006; Leng et al. 2010; Zhou and Zhang 2010). Recently, two zircon U–Pb ages of 14.73±0.13 Ma (2σ) and 12.01±0.29 Ma (2σ) for a quartz monzonite stock and an ore-bearing porphyry, respectively, have been obtained by secondary ion microprobe mass spectrometry (SIMS) (Leng et al. 2010). These ages indicate that the deposit was formed during a post-collision extensional event (30–10 Ma; Chung et al. 2005, 2009) in the Tibetan Orogen. In this study, we present new zircon Hf isotopic compositions, whole-rock geochemical and Sr–Nd–Pb isotopic compositions, and molybdenite Re–Os ages to constrain the magma source of the intrusions and the timing of mineralization, and to further explore their genetic relationship.

Regional geology

The Gangdese porphyry copper belt is located in the Lhasa Terrane (LT) (Fig. 1a), which extends west–eastward for several hundreds of kilometers and is bounded by the Indus-Yarlung suture to the south and the Banggong-Nujiang suture (NBS) to the north. The crystalline basement rocks of the terrane are represented by the Amdo orthogneisses with ages between 530 and 850 Ma (Guynn et al. 2006). They are distributed along the northern margin of this terrane (Harris et al. 1988). The Paleozoic–Mesozoic cover strata are composed of a succession of Ordovician–Triassic shallow marine clastic rocks (Burg and Chen 1984; Kind et al. 1996). The Upper Carboniferous–Lower Permian strata are mainly composed of pyroclastic rocks and carbonate rocks, and crop out in the northern margin of the terrane (Yin and Harrison 2000). These strata are considered to have resulted from the opening of the Nujiang oceanic basin (Pearce and Mei 1988; Gaetani and Garzanti 1991). During the Early Jurassic to the Late Cretaceous, the Neotethyan oceanic crust subducted northwards beneath the Lhasa terrane (Chu et al. 2006; Wen et al. 2008; Ji et al. 2009), forming Andean-type granitoid batholiths and the Xigaze forearc basin (Allègre et al. 1984; Harrison et al. 1992; Durr 1996). Subsequently, the voluminous Gangdese collisional granitoid batholiths were emplaced, and the Paleocene–Eocene Linzizong calc-alkaline volcanic magmas were erupted in the southern LT during collision between the Indian and Asian plates (~65 to 40 Ma) (Dong et al. 2005; Mo et al. 2007, 2008, 2009; Ji et al. 2009; Gao et al. 2010). The post-subduction magmatism in the LT comprises a mid-Miocene potassic igneous belt extending for about 1.500 km, sub-parallel to the Gangdese range. This potassic igneous belt consists mainly of potassic calc-alkaline lavas and ultrapotassic lavas (Turner et al. 1993, 1996; Miller et al. 1999; Williams et al. 2001) and adakite-like porphyries (Chung et al. 2003; Hou et al. 2004; Guo et al. 2007).

The Miocene adakite-like porphyries intruded the Gangdese granitoid batholiths and their surrounding

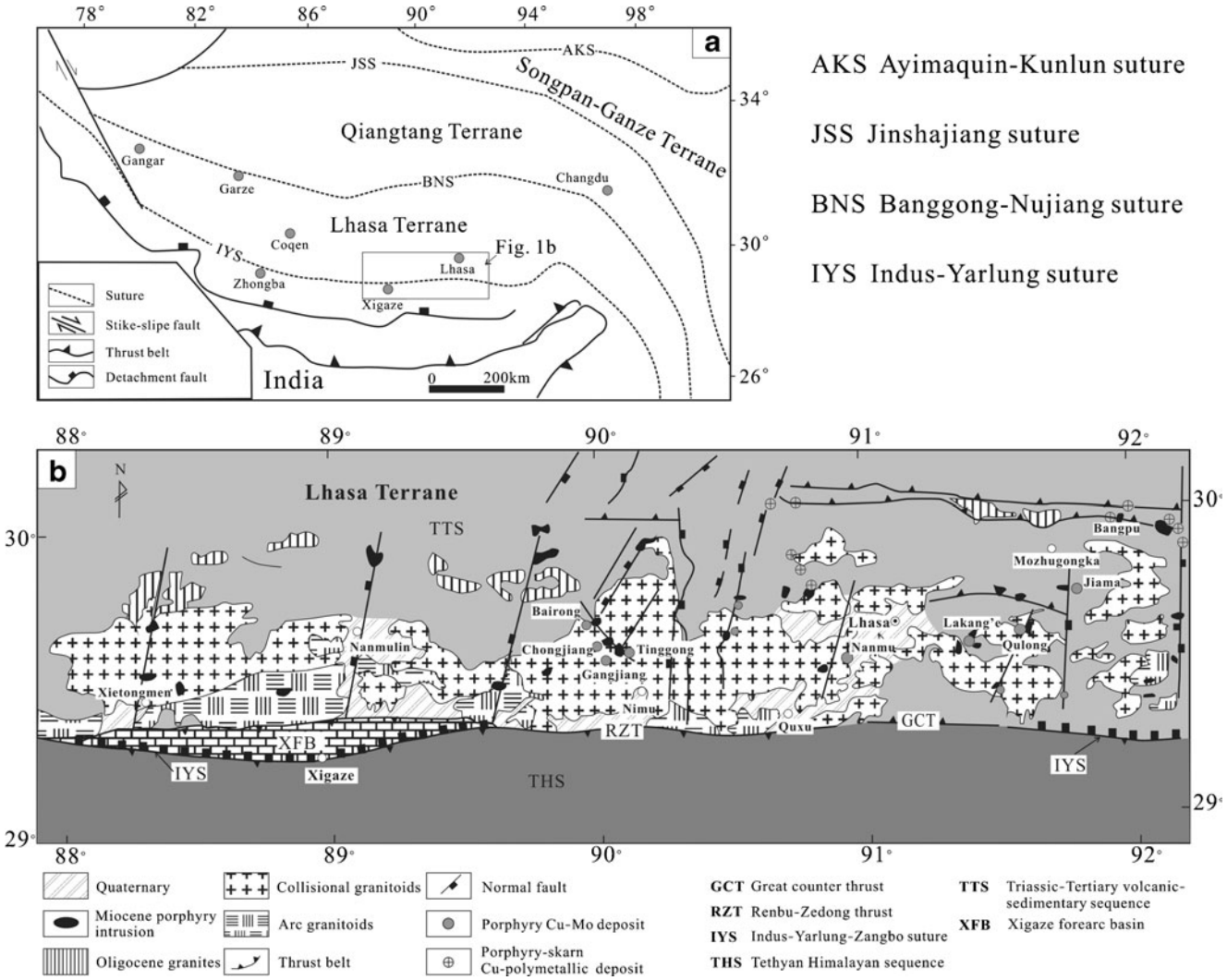

Fig. 1 **a** Simplified tectonic framework of the Himalayan-Tibetan Orogen (Hou et al. 2004) and **b** sketch geological map of the Gangdese porphyry copper belt (modified from Hou et al. 2004, 2009)

Triassic–Tertiary sedimentary sequences as small-volume stocks or dikes. They form a 400-km long, 50-km wide, EW-trending porphyry belt which is bounded by the Renbu-Zedong thrust (Fig. 1). Most age results, obtained by zircon U–Pb, K–Ar, and $^{40}Ar/^{39}Ar$ dating methods (Chung et al. 2003; Rui et al. 2003, 2004; Hou et al. 2004; Qu et al. 2007; Li et al. 2007, 2011), indicate that these porphyries were emplaced between ca. 26 and 10 Ma. Similar $^{40}Ar/^{39}Ar$ ages have been reported for the post-subduction potassic and ultrapotassic lavas in both southern and northern Tibet and southern Karakorum (Coulon et al. 1986; Turner et al. 1993; Miller et al. 1999; Maheo et al. 2002; Chung et al. 2005). Most studies indicate that emplacement of the post-subduction magmatism was controlled by the N–S-striking normal fault systems that were probably formed between 18 and 13 Ma (Yin et al. 1994; Coleman and Hodges 1995; Williams et al. 2001).

Deposit geology

The Gangjiang porphyry Cu–Mo deposit is located in Nimu County, 115 km west of Lhasa City, centered at about 90°E and 29.5°N (Fig. 1b). At present, more than three large-sized porphyry Cu deposits (Chongjiang, Tinggong, and Bairong) have been discovered in the Nimu ore field (Wang et al. 2002; Li et al. 2007; Hou et al. 2009), which are all located in the central region of the GPCB. Three main lithologic units are developed in the Nimu ore field (Wang et al. 2002; Hou et al. 2009). They include: a late Cretaceous sedimentary sequence, consisting of siltstone, mudstone, and overlying greywacke and muddy limestone; a Paleocene–Oligocene volcano- sedimentary sequence (Linzizong volcanic rcoks), consisting of andesitic–dacitic lavas, welded tuffaceous rocks and tuffaceous sandstone; and a Paleocene–

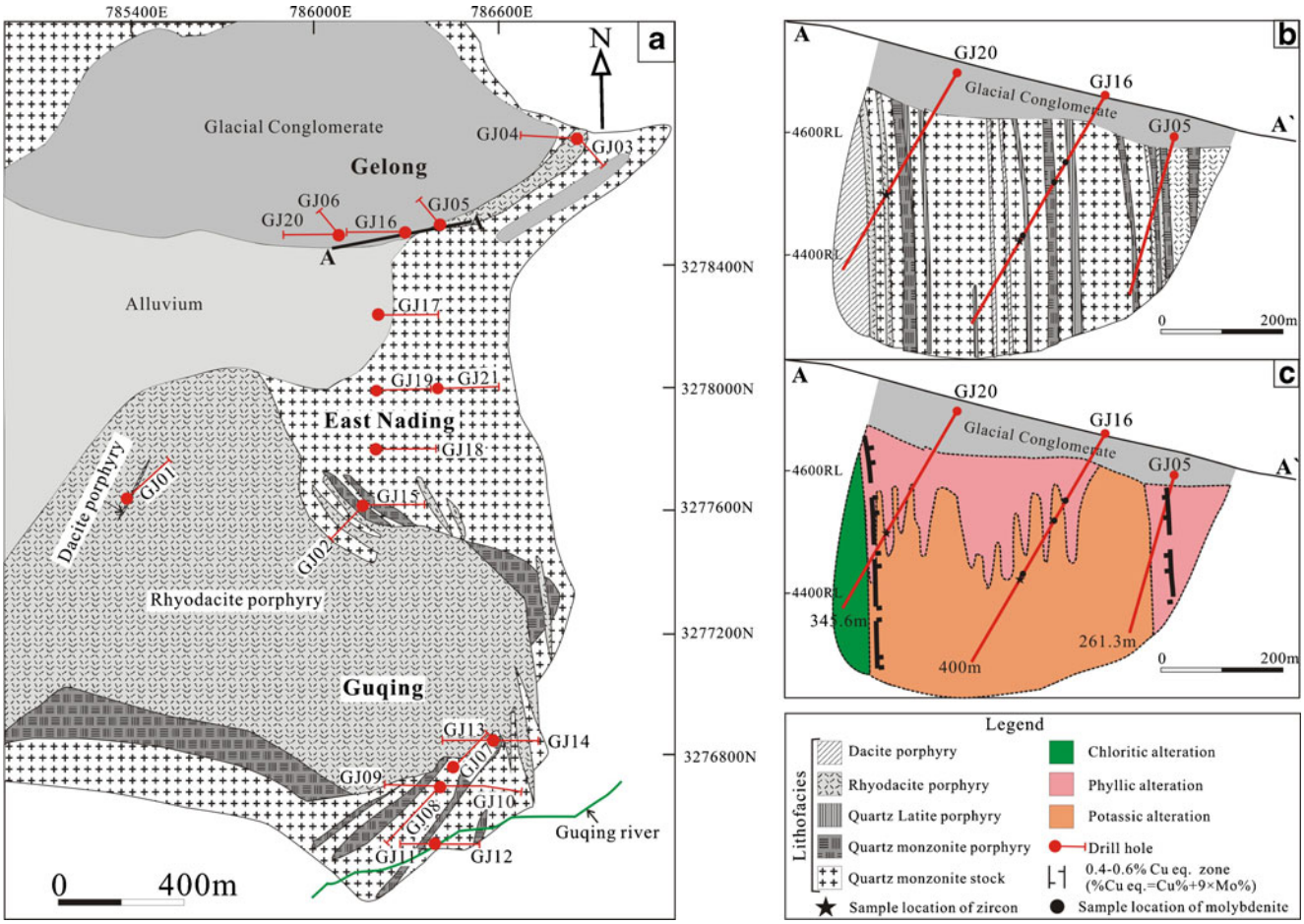

Fig. 2 **a** Simplified geological map of the Gangjiang porphyry Cu–Mo deposit, **b** cross-section along drill holes GJ16, 20 and GJ05, and **c** hydrothermal alteration zones of this cross-section (modified from GGG 2008b and Leng et al. 2010)

Miocene multiphase intrusion, mainly consisting of biotite monzogranite, quartz monzonite, granite porphyry, granodiorite, and quartz diorite.

Lithology of the Gangjiang multiple intrusion

In the Gangjiang deposit, based on detailed mapping and drill core logging, five intrusions with related mineralization and alteration have been recognized (Fig. 2). From the oldest to the youngest, they are quartz monzonite stock (QM), quartz monzonite porphyry (QMP), quartz latite porphyry (QLP), rhyodacite porphyry (RP), and dacite porphyry (DP) (Fig. 3a–d). Several types of breccias (Fig. 3e, f), including magmatic hydrothermal breccias and phreatic breccias, are also developed in this district.

The QM covers an area of ca. 50 km^2 and it is crosscut by late porphyries. It consists mainly of coarse-grained alkali feldspar (25–30 %), plagioclase (30–40 %), quartz (15–20 %), and biotite (5–10 %), with flesh pink color and phanerocrystalline texture. Its accessory minerals are dominated by zircon, apatite, magnetite, and rutile.

The quartz monzonite porphyry occurs as stocks and dikes with widths of <5 to 1,500 m. It intrudes the QM but is crosscut by the rhyodacite and dacite porphyries. It is distinctive from the QM by its porphyritic texture. The QMP contains about 35 to 45 % of phenocrysts which consist

Fig. 3 Photographs of intrusive rocks at Gangjiang porphyry Cu–Mo deposit. **a** potassic altered quartz monzonite; **b** potassic altered quartz latite porphyry; **c** quartz monzonite porphyry cut by the rhyodacite porphyry; **d** weakly chloritic-altered rhyodacite porphyry; **e** magmatic hydrothermal breccia, in which there is one partly rounded quartz monzonite porphyry fragment containing resorbed oval quartz in a matrix of rhyodacite porphyry; **f** phreatic breccia, in which various rock and mineral clasts cemented by chalcedonic matrix; **g** veinlet of quartz–K-feldspar–molybdenite in potassic altered quartz monzonite; **h** vein of quartz–molybdenite–chalcopyrite in potassic altered quartz monzonite; **i** veinlet of quartz–K-feldspar–molybdenite in potassic altered quartz monzonite porphyry; **j** vein of quartz–sericite–molybdenite–chalcopyrite in potassic and strongly phyllic altered quartz monzonite; **k** molybdenite blebs and chalcopyrite disseminated in potassic altered quartz monzonite; **l** outcrop of the copper oxide zone. Abbreviations: *Bi* secondary biotite, *Cpy* chalcopyrite, *Kf* K-feldspar, *Moly* molybdenite, *Pl* plagioclase, *Py* pyrite, *Qz* quartz, *QMP* quartz monzonite porphyry, *RP* rhyodacite porphyry, *Se* Sericite

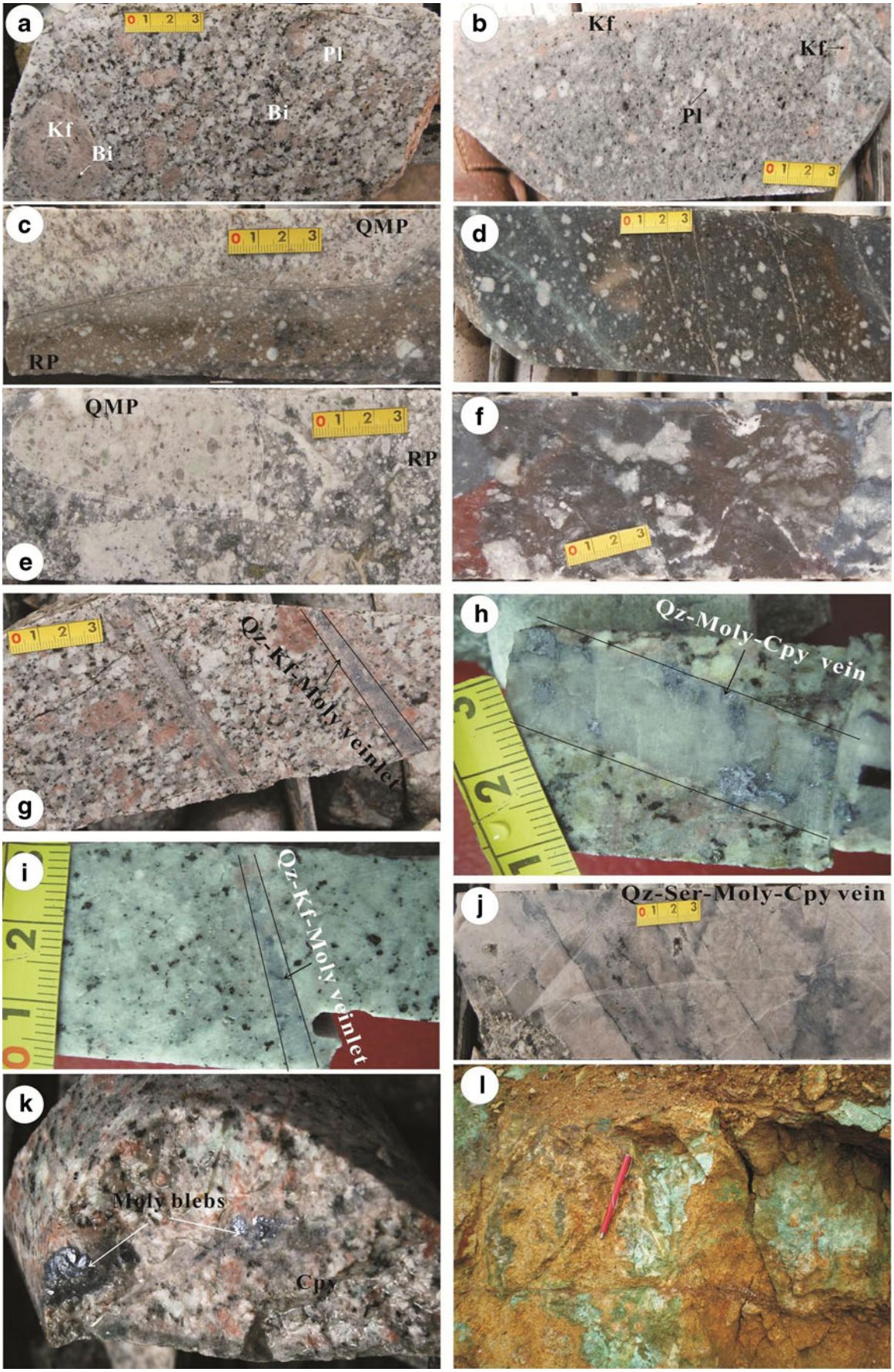
a
Pl
Bi
Kf
Bi
b
Kf
Kf
Pl
c
QMP
RP
d
QMP
RP
e
f
g
Qz-Kf-Moly veinlet
h
Qz-Moly-Cpy vein
i
Qz-Kf-Moly veinlet
j
Qz-Ser-Moly-Cpy vein
k
Moly blebs
Cpy
l

mainly of coarse-grained K-feldspar (15–20 %), plagioclase (10–15 %), quartz (~5 %), and biotite (5–10 %). Its groundmass is composed of quartz and feldspar with fine- to micrograniular texture.

The quartz latite porphyry only occurs as dikes with widths of 1–20 m. It also intrudes the QM, but is crosscut by the rhyodacite and dacite porphyries. It contains fewer and smaller phenocrysts, compared to the QMP. It contains about 15 to 25 % of phenocrysts which consist mainly of coarse-grained K-feldspar (5–10 %), plagioclase (8–12 %), quartz (~3 %), and biotite (~5 %).

The rhyodacite porphyry occurs as stocks and dikes with widths of 1–1,000 m, and intrudes earlier intrusions. It contains about 20–30 % phenocrysts which consist of plagioclase (10–15 %), quartz (5–8 %), biotite (~5 %), and lesser amphibole (~3 %), with porphyritic texture. Its groundmass consists of micro-granular quartz and K-feldspar. Accessory minerals are zircon, apatite, and rutile.

The dacite porphyry is the latest intrusion phase in the deposit area. It occurs as dikes with widths ranging from <1 to 20 m. It contains about 10–20 % phenocrysts which consist mainly of plagioclase (5–10 %), biotite (~5 %), amphibole (~3 %), and minor quartz, with vitrophyric texture. Its groundmass consists of micro-granular quartz, feldspar, and mafic minerals.

Magmatic hydrothermal breccias are well developed in the deposit area (e.g., drill holes GJ08, GJ11, and GJ13). They are composed of partly resorbed and rounded QMP fragments, which contain resorbed rounded quartz phenocrysts, and matrix of the RP (Fig. 3e). Phreatic breccias are distinguished from magmatic hydrothermal breccias by various rock clasts cemented by chalcedonic matrix (Fig. 3f).

Hydrothermal alteration

In the Gangjiang district, many types of hydrothermal alteration have been identified. They include potassic, silicic, phyllic, chloritic, and argillic alterations (Fig. 3a–d). The alteration zones of the mineralized porphyry bodies are similar to those of other porphyry Cu deposits in the GPCB (e.g., Hou et al. 2009; Yang et al. 2009). Potassic, phyllic, and chloritic alteration zones are distributed from the center to the outer part of the porphyry bodies (Fig. 2c).

K-silicate alteration is mainly observed in the QM, QMP, and QLP (e.g., Fig. 3a, b, g). It is represented by pervasively developed potassic mineral assemblages and veinlets and veins of K-feldspar and quartz in the porphyries. The potassic alteration mineral assemblages consist mainly of K-feldspar, secondary biotite, quartz, magnetite, chlorite, and minor anhydrite. The original igneous textures in this zone have been partially destroyed as the original phenocrysts of plagioclase and biotite have been locally replaced by K-feldspar and secondary biotite, respectively.

Phyllic alteration occurs in all porphyry units. Its intensity is stronger in the RP and QMP than in the others in the deposit (Fig. 3c, e). It is characterized by a pervasive replacement of the original minerals of the porphyry by sericite, quartz, pyrite, illite, and chlorite, or was metasomatized to form alteration halos around quartz–sulfides veins. This alteration zone usually overprints the early-formed potassic alteration zone.

Argillic alteration is represented by the development of clay minerals including illite, smectite, kaolinite, and minor alunite. It is only observed in late faults and fractures in the deposit, and is probably resulted from supergene alteration.

Chloritic alteration is characterized by pervasive replacement of most mafic minerals by chlorite and calcite without epidote, distinctive from the propylitic alteration which is common in other porphyry deposits, but not in the Gangjiang district (Leng et al. 2010). The chloritic alteration occurs in all the intrusive rocks and is locally overprinted by weak to moderate phyllic alteration.

Mineralization

The copper and molybdenum mineralization occurs mainly where the potassic and phyllic alteration zones overlap in the quartz monzonite stock (QM), close to the rhyodacite porphyry (RP) (Fig. 2). Three primary orebodies including the Guqing, East Nading, and Gelong have been delineated by trenching and drilling since 2008 (GGG 2009) (Fig. 2a). At Guqing, the mineralized area is about 400 m long by 300 m wide and up to 50 m thick. Between East Nading and Gelong, the mineralized area is about 1 km long by 700 m wide with depths from surface up to 576 m. Supergene copper oxide zones are well developed, with thicknesses of about 60 to 80 m locally. The soluble Cu content of these oxide zones varies from 0.41 to 0.91 % (GGG 2008a). All the copper oxide zones also contain substantial amounts of Mo and Ag, with grades ranging from 0.01 to 0.04 % for Mo and <1 to 30 ppm for Ag, respectively (GGG 2008a). Hypogene sulfide minerals comprise chalcopyrite, molybdenite, and pyrite, with minor bornite, sphalerite, and galena. Supergene minerals in the oxide zone consist of malachite, covellite, neotocite, and limonite. Gangue minerals include quartz, K-feldspar, biotite, sericite, illite, chlorite, calcite, and minor gypsum.

Various styles of mineralization, such as disseminations and patches, veinlets, stockwork veins, vein breccias, and coarse quartz–molybdenite–chalcopyrite veins (Fig.3e, g–k) have been identified in the deposit. Disseminated mineralization mainly occurs in the QM, and is intimately associated with early K-silicate alteration and quartz±K-feldspar–sulfide veinlets (Fig. 3g). No economic orebody was formed at this stage of mineralization because the average grades in the potassic zone are usually lower than 0.1 % for Cu and 0.01 % for Mo, respectively. Late-stage mineralization was

mostly associated with phyllic alteration, and is characterized by quartz–pyrite–chalcopyrite±molybdenite stockwork veins with pyrite more than chalcopyrite in the QM, QMP, and RP. The overprint of these stockwork veins on the early-formed disseminated and veinlet ores resulted in the upgrade of copper and molybdenum contents, and the formation of economic orebodies in the potassic alteration zone overprinted by phyllic alteration. The malachite and covellite patches are mainly hosted in the oxide zones and some vein breccias. It is worth noting that some 10- to 150-cm-wide coarse quartz veins containing abundant molybdenite and minor chalcopyrite have been observed in drill cores GJ15 and GJ16 (Fig. 3j). These veins were probably associated with strong silicic alteration and overprinted by phyllic alteration, and may represent the core of the hydrothermal alteration system. However, they are distinctive from the barren quartz veins in other porphyry deposits (e.g., Bajo de la Alumbrera in Argentina; Ulrich et al. 2002) due to their Mo and Cu mineralization. No intensive mineralization is associated with chloritic and argillic alteration in this deposit.

Analytical methods

Molybdenite Re–Os analytical methods

Four molybdenite samples collected from two drill holes were chosen for Re–Os isotopic dating (Fig. 2, 3). The GJ16-114m molybdenite sample was separated from a potassic altered QM hand specimen, which contains quartz–molybdenite veinlets (Fig. 3g). GJ16-239.4m molybdenite sample was selected from a strongly potassic and phyllic altered QM specimen, which contains a 1-cm-thick quartz–molybdenite–chalcopyrite vein (Fig. 3h). The GJ15-301m molybdenite sample was separated from a coarse quartz–molybdenite–chalcopyrite vein (Fig. 3j) in the potassic altered QM overprinted by strong phyllic and silicic alteration. And the GJ16-139m molybdenite sample was collected from quartz–K-feldspar–molybdenite veinlets in potassic altered QMP (Fig. 3i). Froth flotation was applied first to separate molybdenite from the finely crushed mineralized rocks. Then molybdenite grains were handpicked individually under a binocular microscope to get over 99 % pure molybdenite separates.

Re–Os isotope analysis was performed on a Thermo ICP-MS (TJA X-series) in the Re–Os Laboratory, National Research Center of Geoanalysis, Chinese Academy of Geological Sciences in Beijing. The detailed analytical procedures are described by Du et al. (1994, 2004). A model age of 139.5±2.0 Ma, which is identical to the certified value of 139.6±3.8 Ma (Du et al. 2004), for the molybdenite standard GBW04436 has been obtained in this analysis. Blanks during these analyses are 2.9±0.9 pg for Re and 0.1 pg for Os. The ^{187}Re decay constant of 1.666×10^{-11} year^{-1} (Smoliar et al. 1996) is used to calculate the molybdenite model ages. Uncertainty in Re–Os model ages includes 1.02 % uncertainty in the ^{187}Re decay constant and uncertainty in Re and Os concentrations which comprises weighing errors for both spike and sample, uncertainty in spike calibration and mass spectrometry analytical error.

Major and trace elements, and Sr–Nd–Pb isotope analyses

Based on petrographic observation, the least altered porphyry samples collected from several drill holes were chosen for analyzing major elements, trace elements, and Sr–Nd–Pb isotopes. Major elements were analyzed by using conventional wet chemical methods at the State Key Laboratory of Ore Deposit Geochemistry (SKLODG), Institute of Geochemistry, Chinese Academy of Sciences. The analytical precision is generally better than five relative percent for major elements. Trace elements were analyzed by using a Perkin-Elmer Sciex ELAN DRC-e ICP-MS at the SKLODG. Powdered samples (50 mg) were dissolved in high-pressure Teflon bombs using a HF+HNO_3 mixture for 48 h at ~190 °C. Rhodium was used as an internal standard to monitor signal drift during counting. The international standards GBPG-1, OU-6, and the Chinese National standards GSR-1 and GSR-3 were used for analytical quality control (Qi et al. 2000). The analytical precision is generally better than 10 relative percent for trace elements.

Whole-rock Sr–Nd–Pb isotopic data were obtained on an IsoProbe-T thermal ionization mass spectrometer (TIMS) at Analytical Laboratory of the Beijing Research Institute of Uranium Geology. The mass fractionation corrections for Sr and Nd isotopic ratios are based on an ^{86}Sr/^{88}Sr ratio of 0.1194 and ^{146}Nd/^{144}Nd ratio of 0.7219, respectively. The ^{87}Sr/^{86}Sr ratio of the Standard NBS987 and ^{143}Nd/^{144}Nd ratio of the Standard SHINESTU Nd determined during this study were 0.710250±0.000007 (2σ) and 0.512118± 0.000003 (2σ), respectively. Pb was separated and purified by a conventional cation-exchange technique (AG1×8, 200–400 resin) with diluted HBr used as eluant. The ^{208}Pb/^{206}Pb, ^{207}Pb/^{206}Pb and ^{204}Pb/^{206}Pb ratios of the Standard NBS981 were 2.1681±0.0008 (2σ), 0.91464± 0.00033 (2σ), and 0.059042 ±0.000037 (2σ), respectively.

In situ zircon Hf analysis

Two ore-bearing porphyry samples (GJ16-247.1, GJ16-208) which were dated previously by using SIMS zircon U–Pb dating (Leng et al. 2010) were selected for zircon Hf isotopic analysis. Zircon Lu–Hf isotopic analyses were carried out on the same spots used for previous dating by using a

Table 1 Re–Os data for molybdenite from the Gangjiang porphyry Cu–Mo deposit

Sample	Weight (g)	Re (ppm)		^{187}Re (ppm)		^{187}Os (ppb)		Model age (Ma)	
		Measured	±2σ	Measured	±2σ	Measured	±2σ	Measured	±2σ
GJ16-114m	0.01029	33.98	0.25	21.36	0.16	4.557	0.041	12.81	0.18
GJ16-239.4m	0.01094	86.59	0.70	54.43	0.44	11.65	0.10	12.85	0.18
GJ15-301m	0.03335	37.51	0.28	23.58	0.18	5.045	0.049	12.84	0.19
GJ16-139m	0.05085	69.78	0.60	43.86	0.38	9.142	0.081	12.51	0.19

Neptune multi-collector ICP-MS equipped with a Geolas-193 laser-ablation system at the Institute of Geology and Geophysics, Chinese Academy of Sciences in Beijing (IGGCAS). The detailed instrumental conditions and analytical procedures are similar to those described by Wu et al. (2006). During the course of this study, a weighted mean $^{176}Hf/^{177}Hf$ ratio of 0.282516±5 (2σ) was obtained for the Standard Mud Tank of zircon, which is in good agreement with the reported $^{176}Hf/^{177}Hf$ ratios of 0.282507±6 (2σ) from solution analysis by Woodhead and Hergt (2005) and of 0.282523±43 (2σ) from in situ analysis by Griffin et al. (2006). Initial Hf isotope ratios are calculated with reference to the chondritic reservoir at the time of magma crystallization, which is represented by the age of zircon growth from magma. A decay constant for ^{176}Lu of 1.865×10^{-11} year^{-1} (Scherer et al. 2001), and the chondritic ratios of 0.282772 for $^{176}Hf/^{177}Hf$ and 0.0332 for $^{176}Lu/^{177}Hf$ (Blichert-Toft and Albarede 1997) have been adopted for this study. These values are reported relative to the $^{176}Hf/^{177}Hf$ ratio of 0.282163 for the Standard JMC475. Single-stage model ages (T_{DM1}) are calculated by using the measured $^{176}Lu/^{177}Hf$ ratios, referring to a model depleted mantle with a present-day $^{176}Hf/^{177}Hf$ ratio of 0.28325, which is similar to that of average MORB (Nowell et al. 1998) and $^{176}Lu/^{177}Hf$ ratio of 0.0384 (Griffin et al. 2002). This is similar, though not identical, to the depleted mantle curve defined by juvenile rocks through time (Vervoort and Blichert-Toft 1999). Two-stage model ages (T_{DM2}) are calculated for the source of magma by assuming a mean $^{176}Lu/^{177}Hf$ value of 0.015 for the average continental crust (Griffin et al. 2002).

Results

Re–Os ages of molybdenite

The Re, Os contents and isotopic values of four molybdenite samples from the Gangjiang porphyry Cu–Mo deposit are listed in Table 1. Total Re and ^{187}Os concentrations vary from 33.98 to 86.59 ppm and 4.56 to 11.65 ppb, respectively. The Re–Os model ages of three molybdenite samples from the potassic altered QM samples vary from 12.81±0.18 to 12.85±0.18 Ma, with a weighted average age of 12.83±0.11 Ma (2σ, MSWD=0.053) (Fig. 4). However, a slightly younger Re–Os model age (12.51±0.19 Ma) was obtained for the molybdenite from the potassic altered QMP sample (Fig. 2).

Major and trace elements, and Sr–Nd–Pb isotopic compositions

Rocks of the Gangjiang intrusion have SiO_2 contents varying from 63.5 to 69.4 %, Al_2O_3 from 13.9 to 17.4 %, FeO from 1.76 to 4.12 %, and MgO from 0.62 to 2.18 % (Table 2). Their total alkali concentrations (Na_2O+K_2O) vary from 6.71 to 8.00 wt% with K_2O/Na_2O (wt%) ratios varying from 0.67 to 0.98. Most of them plot within the high-K calc-alkaline field in the diagram of K_2O versus SiO_2. All the samples are characterized by high Sr contents (599–846 ppm), Sr/Y ratios (45–132), and low contents of Y (5.34–17.2 ppm) and heavy rare earth elements (HREE) (e.g., Yb varing from 0.48 to 1.09 ppm). These geochemical features are similar to those of adakites defined by Defant and Drummond (1990) and Martin (1999). The rocks have similar chondrite-normalized rare earth elements (REE) distribution patterns (Fig. 5a), characterized by strong

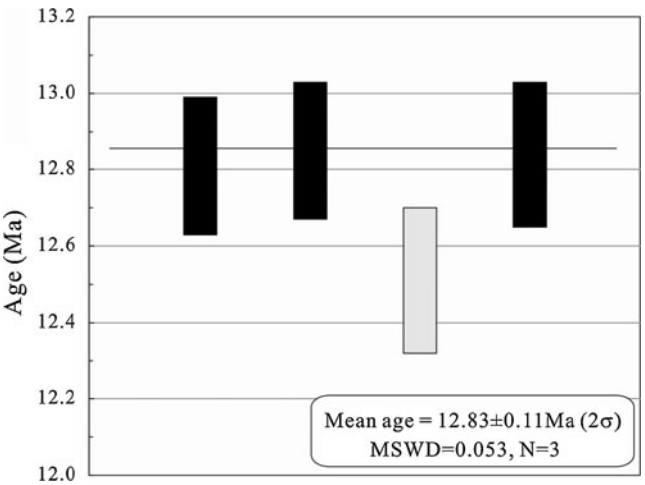

Fig. 4 Re–Os weighted average model age diagram for the molybdenite samples from the Gangjiang deposit

Table 2 Major(in weight percent)and trace element(in ppm)compositions of intrusive rocks from the Gangjiang porphyry Cu–Mo deposit

Sample	GJ10-489.7	GJ10-505	GJ15-466	GJ16-139	GJ19-118.9	GJ13-269	GJ19-143.4
Lithology	QM	QM	QM	QMP	QLP	RP	DP
SiO_2	67.63	69.38	67.76	68.9	69.23	67.67	63.48
Al_2O_3	14.00	15.56	15.40	16.31	17.20	13.92	17.37
FeO	4.12	2.35	2.82	1.76	1.8	2.67	3.84
Fe_2O_3	1.56	1.02	1.36	0.85	0.88	1.26	1.52
CaO	2.32	2.01	2.03	1.88	1.31	2.43	2.26
MgO	0.74	0.62	1.15	0.78	0.76	1.09	2.18
K_2O	3.88	3.00	3.97	3.68	3.58	3.59	2.69
Na_2O	4.12	4.23	4.05	4.32	4.17	4.83	4.02
MnO	0.33	0.17	0.21	0.15	0.14	0.21	0.19
TiO_2	0.27	0.33	0.32	0.41	0.37	0.30	0.34
P_2O_5	0.06	0.06	0.05	0.04	0.04	0.05	0.06
LOI	0.77	1.11	0.94	0.66	0.43	1.76	2.10
Total	99.80	99.84	100.06	99.74	99.91	99.78	100.05
Mg#	24.3	32.0	42.1	44.2	43.0	42.2	50.3
La	30.1	21.4	41.9	22.5	16.9	23.5	46.1
Ce	55.8	40.2	73.4	41.6	33.2	43.5	85.9
Pr	6.40	4.71	8.29	4.70	3.92	5.03	11.1
Nd	23.8	17.8	31.9	17.2	15.2	19.0	44.2
Sm	3.77	2.97	5.32	2.90	2.75	3.31	7.35
Eu	0.77	0.73	1.00	0.66	0.60	0.73	1.25
Gd	2.41	1.94	2.96	1.63	1.63	1.91	4.24
Tb	0.34	0.27	0.43	0.24	0.24	0.29	0.60
Dy	1.40	1.20	1.85	1.06	0.99	1.22	2.63
Ho	0.29	0.24	0.34	0.21	0.18	0.24	0.52
Er	0.80	0.65	0.93	0.59	0.55	0.65	1.36
Tm	0.11	0.09	0.12	0.08	0.08	0.09	0.18
Yb	0.70	0.56	0.86	0.48	0.52	0.56	1.09
Lu	0.10	0.09	0.13	0.07	0.08	0.10	0.16
Li	22.0	23.5	25.7	18.8	21.3	32.6	51.7
Be	3.16	3.70	5.07	3.01	3.10	3.12	3.82
Sc	8.43	4.23	6.38	8.81	5.08	5.11	11.4
V	47.7	47.6	63.4	59.1	38.2	51.9	90.3
Cr	59.5	38.8	56.0	31.2	30.1	50.8	132
Co	9.52	6.80	8.58	5.80	4.96	7.50	11.7
Ni	21.1	15.2	19.3	14.3	12.5	20.3	62.5
Cu	87.8	773	407	617	403	64.2	692
Zn	52.1	40.5	43.3	21.6	73.7	43.6	110
Ga	22.6	21.4	21.8	19.6	20.2	22.5	23.4
Rb	210	171	303	159	158	189	252
Sr	741	846	695	671	599	618	773
Y	7.31	6.41	9.35	5.71	5.34	6.24	17.2
Zr	137	105	138	97.4	119	104	143
Nb	7.62	5.27	8.25	5.31	5.82	5.38	5.67
Mo	7.03	90.1	26.0	147	17.4	3.30	43.5
Ag	0.56	0.67	0.83	0.60	0.52	0.51	0.55
Sn	4.81	2.38	2.59	1.51	1.81	2.13	4.59
Sb	4.59	0.85	0.83	0.73	0.57	1.10	1.32
Cs	18.8	12.9	16.1	10.3	9.46	20.0	27.4

Table 2 (continued)

Sample	GJ10-489.7	GJ10-505	GJ15-466	GJ16-139	GJ19-118.9	GJ13-269	GJ19-143.4
Ba	1090	649	861	943	820	778	778
Hf	3.81	3.02	3.91	2.84	3.46	3.02	4.15
Ta	0.58	0.42	0.69	0.38	0.48	0.44	0.42
Pb	31.8	27.1	36.8	34.3	39.6	37.1	40.3
Th	20.8	14.9	33.2	14.6	15.0	16.4	14.4
U	6.41	3.91	7.00	3.03	2.67	3.67	4.50

Mg#=Mg/(Mg+Fe^{2+})

enrichments of light REE with the La_N/Yb_N ratios of 23.13 to 35.11 and Eu/*Eu values of 0.68 to 0.93. They show strong enrichment in large ion lithophile elements relative to high-field-strength elements (HFSE) with positive anomalies of K, Pb, Th, and U and negative anomalies of Nb, Ta, and Ti in the primitive mantle-normalized trace-element patterns (Fig. 5b).

The Sr, Nd, and Pb isotopic compositions of the analyzed samples are given in Table 3. The samples have high initial $^{87}Sr/^{86}Sr$ ratios varying from 0.7052 to 0.7059, and low $(^{143}Nd/^{144}Nd)_i$ ratios varying from 0.512424 to 0.512542, corresponding to $\varepsilon_{Nd}(t)$ values varying from −3.83 to −1.52, in comparison to the Chondritic Uniform Reservoir (Fig. 6a). The Nd model ages relative to the depleted mantle (DM) range from 835 to 976 Ma. All samples have similar Pb isotope compositions (Table 3), which plot well above the Northern Hemisphere Reference Line (Hart 1984) in the $(^{207}Pb/^{204}Pb)_i$ versus $(^{206}Pb/^{204}Pb)_i$ diagram (Fig. 6b). The initial Pb isotopic ratios are restricted, with the $(^{206}Pb/^{204}Pb)_i$, $(^{207}Pb/^{204}Pb)_i$, and $(^{208}Pb/^{204}Pb)_i$ values varying from 18.242 to 18.468, from 15.607 to 15.625, and from 38.318 to 38.724, respectively.

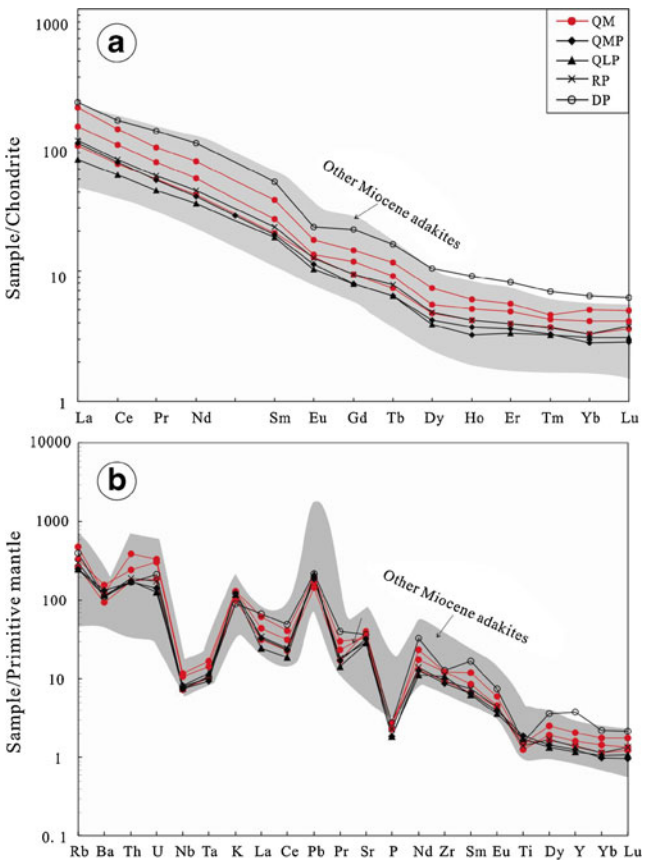

Fig. 5 **a** Chondrite-normalized rare earth element diagram, **b** primitive mantle-normalized incompatible trace-element variation diagram for intrusive rocks from the Gangjiang deposit. The normalizing values are from Sun and McDonough (1989). The published data of Miocene adakites are from Li et al. (2011), Guo et al. (2007), and Chung et al. (2005)

Zircon Hf isotopes

Lu–Hf isotopic data for zircon grains from two samples of GJ16-247.1 (QM) and GJ20-208 (RP) are presented in Table 4. The results are plotted in a diagram of $\varepsilon_{Hf}(t)$ against the $^{206}Pb/^{238}U$ ages (Fig. 7). Previous analyses (Leng et al. 2010) show that zircon grains from the QM sample GJ16–247.1 have U–Pb ages ranging from 14.2 to 15.4 Ma (Table 4), with a weighted mean $^{206}Pb/^{238}U$ age of 14.73± 0.13 Ma (2σ, MSWD=1.3, n=16), representing its crystallization age (Leng et al. 2010). However, a weighted mean $^{206}Pb/^{238}U$ age of 12.01±0.29 Ma (2σ, MSWD=2.3, n=8), representing the crystallization age, for the RP sample GJ20–208 sample has been obtained, although some older ages of 13.3–14.58 and 55.5 Ma for inherited zircons have also been obtained (Leng et al. 2010).

Sixteen spot analyses of Lu–Hf isotopes were made on 16 zircon grains from the quartz monzonite sample. The $\varepsilon_{Hf}(t)$ values are positive and vary over a limited range from +2.25 to +4.57 with an average value of +3.33 (Table 4). Their corresponding crustal model ages (T_{DM2}) vary from 806 to 955 Ma with an average of 886 Ma (Table 4; Fig. 7b). Seventeen in situ analyses of Lu-Hf isotopes were done on 17 zircon grains, including six inherited zircon grains, from the rhyodacite porphyry sample. The $\varepsilon_{Hf}(t)$ values for nine grains of magmatic zircon from this sample vary from +5.53 to +7.81 with an average of +6.64, which is higher than that

Table 3 Sr, Nd, and Pb isotopic compositions of intrusive rocks from the Gangjiang porphyry Cu–Mo deposit

Sample	GJ10-489.7	GJ10-505	GJ15-466	GJ16-139	GJ19-118.9	GJ13-269	GJ19-143.4
$^{87}Sr/^{86}Sr$	0.70548	0.70543	0.7061	0.705381	0.705584	0.705355	0.705406
$\pm 2\sigma$	0.00001	0.000007	0.000007	0.000007	0.000009	0.000009	0.000008
$^{143}Nd/^{144}Nd$	0.512509	0.512511	0.512433	0.512496	0.512505	0.512552	0.512509
$\pm 2\sigma$	0.000006	0.000006	0.000005	0.000004	0.000006	0.000005	0.000004
$^{208}Pb/^{204}Pb$	38.697	38.693	38.765	38.702	38.642	38.673	38.334
$\pm 2\sigma$	0.004	0.005	0.004	0.004	0.003	0.005	0.004
$^{207}Pb/^{204}Pb$	15.62	15.619	15.626	15.617	15.607	15.616	15.611
$\pm 2\sigma$	0.002	0.002	0.002	0.002	0.001	0.002	0.002
$^{206}Pb/^{204}Pb$	18.473	18.463	18.488	18.473	18.443	18.46	18.253
$\pm 2\sigma$	0.002	0.002	0.002	0.002	0.002	0.003	0.002
$(^{87}Sr/^{86}Sr)i$	0.705320	0.705314	0.705849	0.705245	0.705432	0.705179	0.705219
$(^{143}Nd/^{144}Nd)_i$	0.512500	0.512502	0.512424	0.512487	0.512495	0.512542	0.512500
$\varepsilon_{Nd}(t)$	−2.34	−2.31	−3.83	−2.60	−2.44	−1.52	−2.35
T_{DM} (Ma)	835	871	976	900	952	849	871
$(^{208}Pb/^{204}Pb)i$	38.667	38.668	38.724	38.683	38.625	38.653	38.318
$(^{207}Pb/^{204}Pb)i$	15.619	15.618	15.625	15.616	15.607	15.615	15.610
$(^{206}Pb/^{204}Pb)i$	18.452	18.448	18.468	18.464	18.436	18.450	18.242

of zircons from the quartz monzonite (sample GJ16-247.1). Corresponding crustal model ages (T_{DM2}) range from 596 to 742 Ma with an average of 671 Ma, which is lower than that of zircons from the GJ16-247.1 (Table 4; Fig. 7b). In addition, the $\varepsilon_{Hf}(t)$ values for several zircons of other populations (13.3–14.58 Ma, n=5) from sample GJ20-208 vary from +4.75 to +6.23, i.e., slightly higher for zircons from sample GJ16-247.1.

Discussion

Timing and duration of the magmatism and mineralization

The timing and duration of the magmatic hydrothermal events are crucially important in understanding ore deposits, from both academic and exploration viewpoints (Stein et al. 1997). Based on published zircon U–Pb dating results (Leng et al. 2010) and the Re–Os radiometric ages for molybdenite obtained in this study, as well as detailed geologic mapping and drill core logging data, the ages of ore-bearing porphyries and associated Cu–Mo mineralization in the Gangjiang Cu–Mo deposit are well constrained.

As noted above, the zircon SIMS U–Pb dating results indicate that the quartz monzonite stock was formed at 14.73±0.13 Ma, while the rhyodacite intruded at 12.01±0.29 Ma (Leng et al. 2010). Therefore, it follows that the QMP and QLP were emplaced between 12 and 15 Ma, although no precise radiometric age has been determined for these porphyries. Because the orebodies were cut by the DP dikes and no copper and molybdenum mineralization has been observed in the DP, it is inferred that the magmatism responsible for the Cu–Mo mineralization could have lasted as long as about 2.7 Ma in the Gangjiang deposit. This is comparable to the duration of porphyry copper formation elsewhere in the GPCB and the central Andes. For example, a range of zircon SHRIMP U–Pb ages from 11.6±0.9 to 16.8±0.8 Ma has been obtained for the multiphase porphyry intrusions from monzogranite to quartz diorite at the Chongjiang deposit in the GPCB (Hou et al. 2004; Rui et al. 2004; Zheng et al. 2004; Qu et al. 2009). Zircon U–Pb ages of 16.0±0.8 Ma for ore-bearing monzogranite porphyry (Li et al. 2011) and 17.0±0.6 Ma for ore-bearing granodiorite porphyry (Rui et al. 2004) at the Tinggong deposit in the GPCB are relatively older than the bulk-rock K–Ar and $^{40}Ar/^{39}Ar$ ages, which range from 12.9±0.5 to 14.9±0.2 Ma, of biotite from ore-bearing porphyries (Li and Rui 2004; Li et al. 2007). In addition, high-precision U–Pb ages of zircons from multiple intrusive rocks of the Quellaveco porphyry Cu–Mo deposit in southern Peru suggest that the porphyry system has been active intermittently for at least 3.25 Ma (Sillitoe and Mortensen 2010). Therefore, a multiple-phase porphyry system with long life spans could be required for the formation of porphyry copper deposits, especially for giant deposits (Barra et al. 2005; Schütte et al. 2012).

Molybdenite Re–Os dating method has become a powerful tool to constrain the ages of mineralization directly, due to the high Re and low common Os concentrations of molybdenite (Stein et al. 1997). In this study, Re–Os model ages obtained for four molybdenite samples from the ore-bearing porphyries

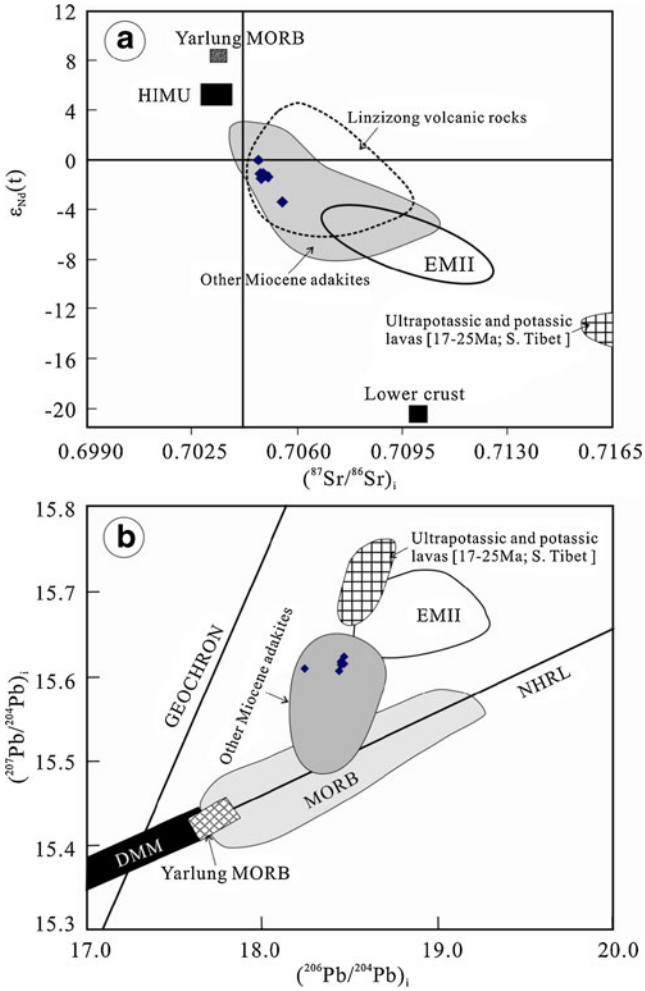

Fig. 6 **a** $^{87}Sr/^{86}Sr$ versus $^{143}Nd/^{144}Nd$ diagram, **b** $^{207}Pb/^{204}Pb$ versus $^{206}Pb/^{204}Pb$ diagram, showing the isotopic signatures for the intrusive rocks from the Gangjiang deposit. Data for the published Miocene porphyries are from Hou et al. (2004), Guo et al. (2007), and Li et al. (2011). Data for Linzizong volcanic rocks are from Zhu et al. (2008) and Mo et al. (2007). Data for ultrapotassic and potassic lavas in southern Tibet are from Turner et al. (1993), Miller et al. (1999), and Ding et al. (2003). Data for Yarlung MORB and Lower crust are from Mahoney et al. (1998) and Miller et al. (1999), respectively. DMM, HIMU and EMII represent three types of mantle end-members (Zinder and Hart 1986)

range from 12.51 to 12.85 Ma. All the Re–Os model ages are significantly younger than that of the quartz monzonite stock, while the youngest Re–Os age of molybdenite (12.51± 0.19 Ma) is just slightly older than that of the rhyodacite porphyry. The small difference between the RP U–Pb zircon age and the molybdenite Re–Os age might be caused by an underestimation of the age uncertainty of the U–Pb age. Highly precise and accurate radiometric dating (e.g., Arribas et al. 1995; Marsh et al. 1997) and numerical simulation (e.g., Cathles et al. 1997) studies suggest that a hydrothermal system sustained by single intrusive porphyry lasts only about 0.01 to 1 Ma. In addition, copper and molybdenum contents in the potassic altered QM are generally lower than 0.1 and 0.01 %, respectively, whereas the Cu and Mo contents of orebodies close to the RP (see Fig. 2) are much higher. Therefore, it is proposed that the RP probably played an important role in upgrading the Cu and Mo mineralization of the early potassic altered QM.

Constraints on the magma source

The geochemical features of ore-bearing intrusive rocks in the Gangjiang deposit are in accordance to those of adakite, and are similar to those of other ore-bearing porphyries in the GPCB (e.g., Gao et al. 2003; Hou et al. 2004, 2009; Li et al. 2011). However, the genesis of these adakite-like porphyries in the GPCB is still poorly constrained as their genetic models remain controversial. Three models have been proposed for adakite-like porphyries: partial melting of (1) thickened mafic lower crust (e.g., Chung et al. 2003; Hou et al. 2004), (2) subducted oceanic crust (e.g., Qu et al. 2004), or (3) metasomatized upper mantle by slab-released melts (Gao et al. 2007). All the studied samples show features of high K_2O contents (varying from 2.69 to 3.97 %), high $(^{87}Sr/^{86}Sr)_i$ ratios (from 0.7052 to 0.7059), relative low Mg# (from 24 to 40), and low $\varepsilon_{Nd}(t)$ values (from −3.83 to −1.52). They are quite distinct from the geochemical features of adakites derived from the partial melting of subducted oceanic crust (Martin 1999). Compared to potassic and ultrapotassic igneous rocks from this region, which have been shown to be derived from partial melting of the lithospheric mantle (Miller et al. 1999; Williams et al. 2001, 2004), the Gangjiang samples are characterized by lower Ni (mostly <20 ppm) and Cr (mostly <60 ppm) contents (Table 2), lower $(^{87}Sr/^{86}Sr)_i$ ratios and higher $\varepsilon_{Nd}(t)$ values (Fig. 6a). Therefore, the first model rather than the latter two models better explains the origin of the ore-bearing porphyries in the Gangjiang district, as also supported by geophysical and geochemical data (cf. Chung et al. 2005, 2009; Hou et al. 2009; and references therein). Likewise, the porphyries in the Gangjing deposit have Sr–Nd–Pb isotopic compositions which are similar to those of the Linzizong volcanic rocks and other adakite-like porphyries in the GPCB (Fig. 6a). Moreover, these ore-bearing porphyries are characterized by high Sr/Y and La/Yb ratios and low Y and HREE contents. This indicates that these porphyries could be derived from a garnet-bearing amphibolite or eclogite, similar to other adakite-like porphyries in the GPCB. Therefore, the newly formed thickened lower crust, which resulted from magma underplating during the Paleocene–Eocene and the subsequent metamorphism of garnet-bearing amphibolite or eclogite during the period 30–45 Ma, could be a source for these adakite-like porphyries (Hou et al. 2009). Nevertheless, the real genetic link between these adakite-like magmas and the Cu–Mo mineralization is still enigmatic. Hou et al. (2004, 2009) proposed that input of

Table 4 In situ Lu–Hf isotopes of zircon separated from samples GJ16-247.1 and GJ20-208 samples in the Gangjiang porphyry Cu–Mo deposit

Spots	Age[a] (Ma)	$^{176}Yb/^{177}Hf$	±2σ	$^{176}Lu/^{177}Hf$	±2σ	$^{176}Hf/^{177}Hf$	±2σ	$\varepsilon_{Hf}(t)$	T_{DM1} (Ma)	T_{DM2} (Ma)
GJ16-247.1 (quartz monzonite)										
1	14.23	0.01347	0.00007	0.000565	0.000002	0.282873	0.000014	3.89	531	849
2	14.27	0.01057	0.00018	0.000474	0.000007	0.282853	0.000013	3.16	558	896
3	14.93	0.01282	0.00009	0.000572	0.000004	0.282854	0.000018	3.22	558	893
4	14.69	0.01469	0.00029	0.000642	0.000013	0.282868	0.000014	3.72	539	861
5	14.66	0.01406	0.00029	0.000619	0.000010	0.282892	0.000016	4.57	505	806
6	14.74	0.01563	0.00034	0.000619	0.000012	0.282835	0.000014	2.53	586	937
7	14.68	0.01147	0.00009	0.000513	0.000002	0.282876	0.000017	3.98	527	844
8	14.77	0.00963	0.00014	0.000425	0.000006	0.282859	0.000014	3.39	549	882
9	14.47	0.01476	0.00030	0.000625	0.000012	0.282836	0.000015	2.57	584	934
10	14.81	0.00983	0.00004	0.000434	0.000002	0.282863	0.000014	3.53	543	873
11	15.08	0.01421	0.00010	0.000614	0.000003	0.282826	0.000014	2.25	597	955
12	14.70	0.01404	0.00016	0.000612	0.000007	0.282860	0.000014	3.44	550	879
13	15.38	0.01434	0.00003	0.000651	0.000001	0.282838	0.000017	2.67	581	928
14	15.00	0.01709	0.00006	0.000704	0.000002	0.282865	0.000013	3.60	545	868
15	14.51	0.01167	0.00004	0.000519	0.000003	0.282858	0.000014	3.36	551	883
16	14.59	0.00973	0.00011	0.000422	0.000005	0.282859	0.000013	3.39	549	882
GJ20-208 (rhyodacite porphyry)										
1	11.74	0.02223	0.00021	0.000860	0.000010	0.282986	0.000019	7.80	376	596
2[b]	14.58	0.01402	0.00016	0.000549	0.000005	0.282898	0.000017	4.75	496	794
3[b]	13.26	0.03230	0.00134	0.001050	0.000035	0.282940	0.000016	6.23	442	698
4[b]	14.34	0.01707	0.00033	0.000624	0.000011	0.282916	0.000018	5.40	472	753
5	11.80	0.01322	0.00038	0.000513	0.000014	0.282960	0.000018	6.92	408	653
6[b]	14.57	0.00845	0.00026	0.000320	0.000008	0.282919	0.000017	5.52	463	745
7	12.54	0.02436	0.00056	0.000929	0.000016	0.282937	0.000018	6.10	446	706
8	11.79	0.03198	0.00030	0.001202	0.000010	0.282962	0.000021	7.32	398	627
9	11.79	0.02559	0.00029	0.000964	0.000008	0.282921	0.000020	5.70	466	731
10	12.03	0.03148	0.00040	0.000990	0.000012	0.282954	0.000023	6.46	433	683
11[b]	55.54	0.03358	0.00150	0.001159	0.000042	0.282972	0.000024	4.47	557	843
12	11.82	0.03941	0.00142	0.001362	0.000046	0.282926	0.000023	6.73	417	665
13[b]	14.41	0.02959	0.00020	0.001116	0.000006	0.282947	0.000023	5.35	472	755
14[c]	–	0.05342	0.00022	0.001648	0.000011	0.282866	0.000020	6.96	414	650
15[c]	–	0.01957	0.00089	0.000694	0.000027	0.282955	0.000020	5.53	468	742
16[c]	–	0.01256	0.00006	0.000516	0.000002	0.282915	0.000021	6.70	422	667
17[c]	–	0.03964	0.00042	0.001333	0.000013	0.282958	0.000021	6.83	420	659

[a] Denotes the zircon 206Pb/238U age from Leng et al. (2010). The initial Hf ratios of the analyzed zircon spots were calculated on the basis of the measured $^{206}Pb/^{238}U$ age, respectively

[b] Zircon grains of other populations

[c] $\varepsilon_{Hf}(t)$ and T_{DM2} values were calculated by using a crystallization age of 12.0 Ma based on the cathodoluminescence images of zircon grains

upper mantle components into the lower crust is a key to the metalliferous properties of these adakite-like magmas, because it can contribute Cu and other metals into the magmatic system, although no convincing evidences were provided. Li et al. (2011) argued that this juvenile lower crust could have inherited the characteristics of arc magma with abundant F, Cl, and Cu and a high oxidation state, which contributed to the formation of porphyry deposits in the GPCB. If this is the case, it is hard to understand why the Paleocene–Eocene intrusions, which were directly derived from the underplated magma, are not associated with Cu–Mo–Au mineralization in the Gangjiang deposit.

Zircon is a resistant and refractory mineral during chemical weathering and partial melting, and can effectively preserve the initial $^{176}Hf/^{177}Hf$ ratios of the igneous host rocks, so their Hf isotopic compositions can be used to trace

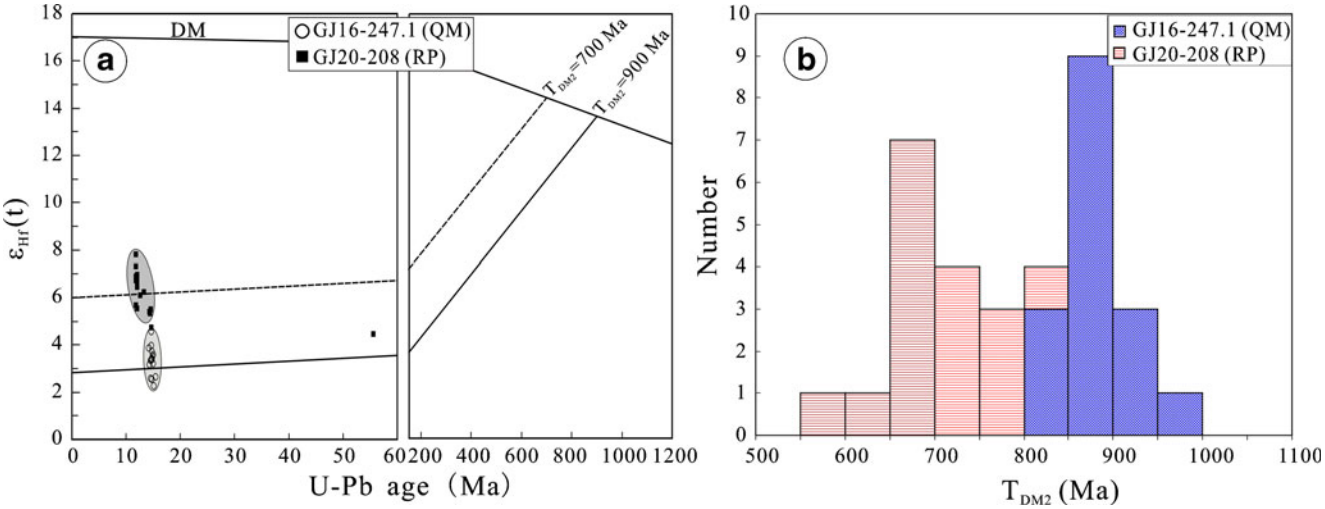

Fig. 7 **a** Plots of $\varepsilon_{Hf}(t)$ values versus U–Pb ages of zircons, **b** histograms of their Hf crustal model ages (T_{DM2})

the magma source (Kinny and Maas 2003). Most studies indicate that zircon Hf isotopic data can be a sensitive and powerful tracer with the potential to provide unique petrogenetic information (Griffin et al. 2002; Hawkesworth and Kemp 2006; Yang et al. 2007). In this study, although the Sr–Nd–Pb isotopic compositions of two ore-bearing porphyries are similar to each other, the Hf isotopic compositions of magmatic zircons from a QM sample (GJ16-247.1), with $\varepsilon_{Hf}(t)$ values ranging from +2.25 to +4.57, are quite different to those, with $\varepsilon_{Hf}(t)$ values varying from +5.53 to +7.81, of zircons from a RP sample (GJ20-208) (Table 4). Moreover, it seems that the zircon $\varepsilon_{Hf}(t)$ values correlate with the emplacement ages, with higher $\varepsilon_{Hf}(t)$ values for the younger RP than those for the older QM stock (Fig. 7a). This elevated radiogenic Hf isotopic feature might be attributed to either the involvement of subducted components (Vervoort and Blichert-Toft 1999; Woodhead et al. 2001; Chauvel et al. 2007) or the input of mantle components (Ji et al. 2009; Mo et al. 2009). If the contribution of subducted sediments in the formation of the magmas increased gradually, the model Hf ages (T_{DM2}) of zircons from the late-formed RP rocks should be older than those of the early-formed QM. However, the measured results do not support this model. Therefore, it is proposed that much more mantle components have contributed to the formation of RP than QM. This suggests that the involvement of mantle components in porphyry formation increased during late stages of magmatism in the Gangjiang igneous complex.

Implications for the tectonic setting of the Gangjiang Cu–Mo deposit

As both the U–Pb ages of zircons and Re–Os ages of molybdenite of ore-bearing porphyries in the Gangjiang deposit are in accordance with the published ages of the post-collision adakite-like porphyries (10–26 Ma) and K-rich magmatic rocks (8–25 Ma) in the Lhasa Terrane (Miller et al. 1999; Williams et al. 2001, 2004; Ding et al. 2003; Chung et al. 2003, 2009; Hou et al. 2004, 2009), we conclude that this deposit was also formed in a post-subduction collisional setting, similar to other porphyry deposits in the GPCB. Two separate prominent geodynamic models have been put forward to explain the generation of the post-subduction magmas. They are the convective lithospheric thinning (delamination) model (Miller et al. 1999; Williams et al. 2001, 2004; Chung et al. 2005) and the subducted slab break-off model (Maheo et al. 2002; Hou et al. 2004, 2009). Ji et al. (2009) argued that the post-subduction magmatism is 20–30 Ma later than the initiation age of the India–Asia collision, thus its genesis cannot be explained by the slab break-off model. Moreover, a linear belt of the distribution of the post-subduction magmatic rocks with a length of more than 1,000 km is also hard to interpret by this model (Li et al. 2011). In addition, the Hf isotopic compositions of zircons from two-stage ore-bearing porphyries in the Gangjiang deposit indicate that the input of mantle components into the porphyry magma source has increased from 14.7 to 12 Ma. This can be easily explained by the convective lithospheric thinning model, rather than the slab break-off model. Therefore, the convective lithospheric thinning model can be used to explain the generation of the post-subduction ore-bearing adakite-like porphyries of the Gangjiang deposit in the GPCB (e.g., Li et al. 2011). Following the onset of "hard collision" between the Indian and Euroasian plates at ~45 Ma, the continuous northward impingement of the Indian plate should have given rise to significant contraction in the lower part of the Lhasa lithosphere that might have been thermally weakened and "softened" by previous arc magmatism (Chung et al. 2005, 2009). Thus, the juvenile lower crust underwent drastic thickening (≥55 km), and then was metamorphosed

into garnet-bearing amphibolite. This high-density lower crust, along with thickened Lhasa lithospheric mantle root, became unstable and began foundering and thinning when the maximum sustainable gravitational load had been reached (Chung et al. 2009). Resultant convective removal of the lower lithosphere root and its replacement by hotter asthenosphere would have raised the geothermal gradient and caused partial melting of the juvenile lower crust to form adakite-like magmas (Chung et al. 2005). Importantly, the upper mantle components either from the lithospheric mantle or the asthenosphere could be inevitably involved in this magmatism, which was accompanied with the convective thinning of the lower lithospheric root. This process has also been proposed by Richards (2009) to decipher the genesis of post-subduction porphyries in collisional settings. Therefore, it is proposed that the Miocene Gangjiang porphyry Cu–Mo deposit (and possibly the Gangdese porphyry copper belt) could be a consequence of the removal of the lithospheric root and the replacement by asthenosphere, following the sudden rise in topography of southern Tibet (Chung et al. 2009).

Conclusions

The Gangjiang porphyry Cu–Mo deposit is a recently discovered deposit in the Gangdese porphyry Cu belt in southern Tibet. Cu and Mo mineralization occurs as disseminations or veins mainly in the overlapping part of the potassic and phyllic alteration zones of quartz monzonite, close to a rhyodacite porphyry stock.

The Re–Os molybdenite ages, along with our previous zircon U–Pb ages indicate that magmatism and Cu–Mo mineralization in the Gangjiang deposit lasted at least about 2.7 and 0.3 Ma, respectively.

The $\varepsilon_{Hf}(t)$ values of magmatic zircons from the late intramineral rhyodacite porphyry (+5.53 to +7.81) are higher than those (+2.25 to +4.57) of the pre-mineral quartz monzonite. This observation indicates that the mantle contribution in magma formation probably increased from 14.7 to 12.0 Ma.

Based on our study and previous works, we propose that the Miocene Gangjiang deposit (and possibly the Gangdese porphyry copper belt) formed as a consequence of the removal of the lithospheric root, and the input of upper mantle components into the porphyry systems, which may have played a key role in the formation of the porphyry deposit in the Tibetan Orogen.

Acknowledgments This study was jointly supported by grants from the Natural Science Foundation of China (41003023 and 40873039), and the Special Fund of the State Key Laboratory of Ore Deposit Geochemistry. Without the practical assistance and cooperation of a number of individuals and organizations, the research described in this paper could not have been completed. In particular, thanks are due to Jinhui Yang and Yueheng Yang of the IGGCAS for analyzing Hf isotopes by using LA-ICP-MS, Jianyong Cui of the Beijing Research Institute of Uranium Geology for analyzing Nd–Sr–Pb isotopes by using TIMS, Shaosong Peng of the SKLODG for analyzing major elements by using conventional wet chemical methods, Jing Hu of the SKLODG for analyzing trace elements by using ICP-MS. Many thanks are also due to Ciceron Jun Angeles, Romeo S. Aquino, Jeffrey Malaihollo, Dong Lan, Ruyi Zhao, and Shuhong Wang for their help and fruitful discussion during field trip and to Wei-Terry Chen for his helpful suggestions and language improvement on early draft of this manuscript. This manuscript also benefited greatly from strict reviews by Jeremy Richards and Fernando Barra. The Editor-in-Chief Bernd Lehmann is also appreciated for his helpful suggestions.

References

Allègre CJ, Courtillot V, Tapponnier P, Hirn A, Mattauer M, Coulon C, Jaeger JJ, Achache J, Scharer U, Marcoux J, Burg JP, Girardeau J, Armijo R, Gariepy C, Gopel C, Li TD, Xiao XC, Chang CF, Li GQ, Lin BY, Teng JW, Wang NW, Chen GM, Han TL, Wang XB, Den WM, Sheng HB, Cao YG, Zhou J, Qiu HR, Bao PS, Wang SC, Wang BX, Zhou YX, Xu RH (1984) Structure and evolution of the Himalaya-Tibet orogenic belt. Nature 307:17–22

Arribas A, Hedenquist JW, Itaya T, Okada T, Concepcion RA, Garcia JS (1995) Contemporaneous formation of adjacent porphyry and epithermal Cu-Au deposits over 300 ka in northern Luzon, Philippines. Geology 23:337–340

Barra F, Ruiz J, Valencia VA, Qchoa-Landín L, Chesley JT, Zurcher L (2005) Laramide porphyry Cu-Mo mineralization in Northern Mexico: age constrains from Re-Os geochrononology in molybdenite. Econ Geol 100:1605–1616

Blichert-Toft J, Albarede F (1997) The Lu-Hf isotope geochemistry of chondrites and the evolution of the mantle-crust system. Earth Planet Sci Lett 148:243–258

Burg JP, Chen GM (1984) Tectonics and structural zonation of Southern Tibet, China. Nature 311:219–223

Cathles LM, Erendi A, Barrie T (1997) How long can a hydrothermal system be sustained by a single intrusive event? Econ Geol 92:766–771

Chauvel C, Lewin E, Carpentier M, Arndt NT, Marini JC (2007) Role of recycled oceanic basalt and sediment in generating the Hf-Nd mantle array. Nat Geosci 1:64–67

Chu MF, Chung SL, Song B, Liu D, O'Reilly SY, Pearson NJ, Ji J, Wen DJ (2006) Zircon U-Pb and Hf isotope constraints on the Mesozoic tectonics and crustal evolution of southern Tibet. Geology 34:745–748

Chung SL, Liu DY, Ji JQ, Chu MF, Lee HY, Wen DJ, Lo CH, Lee TY, Qian Q, Zhang Q (2003) Adakites from continental collision zones: melting of thickened lower crust beneath southern Tibet. Geology 31:1021–1024

Chung SL, Chu MF, Zhang YQ, Xie YW, Lo CH, Lee TY, Lan CY, Li XH, Zhang Q, Wang YZ (2005) Tibetan tectonic evolution inferred from spatial and temporal variations in post-collisional magmatism. Earth Sci Rev 68:173–196

Chung SL, Chu MF, Ji JQ, O'Reilly SY, Pearson NJ, Liu DY, Lee TY, Lo CH (2009) The nature and timing of crustal thickening in Southern Tibet: geochemical and zircon Hf isotopic constraints from postcollisional adakites. Tectonophysics 477:36–48

Coleman M, Hodges K (1995) Evidence for Tibetan plateau uplift before 14 Myr ago from a new minimum age for east–west extension. Nature 374:49–52

Cooke DR, Hollings P, Walshe JL (2005) Giant porphyry deposits: characteristics, distribution, and tectonic controls. Econ Geol 100:801–818

Corbett GJ, Leach TM (1998) Southwest Pacific Rim gold-copper systems: structure, alteration, and mineralization. Soc Econ Geol Sp Pub 6:1–237

Coulon C, Maluski H, Bollinger C, Wang S (1986) Mesozoic and Cenozoic volcanic rocks from central and southern Tibet: ^{39}Ar–^{40}Ar dating, petrological characteristics and geodynamical significance. Earth Planet Sci Lett 79:281–302

Defant MJ, Drummond MS (1990) Derivation of some modern arc magmas by melting of young subducted lithosphere. Nature 347:662–665

Ding L, Kapp P, Zhong DL, Deng WM (2003) Cenozoic volcanism in Tibet: evidence for a transition from oceanic to continental subduction. J Petrol 44:1833–1865

Dong GC, Mo XX, Zhao ZD, Guo TY, Wang LL, Chen T (2005) Geochronologic constraints on the magmatic underplating of the Gangdise belt in the India-Eurasia collision: evidence of SHRIMP II zircon U-Pb dating. Acta Geol Sin-Engl 79:787–794

Du AD, He HY, Yin WN, Zhou XQ, Sun YL, Sun DZ, Chen SZ, Qu WJ (1994) The study on the analytical methods of Re-Os age for molybdenites. Acta Geol Sinica 68:339–347 (in Chinese with English abstract)

Du AD, Wu SQ, Sun DZ, Wang SX, Qu WQ, Markey R, Stain H, Morgan J, Malinovskiy D (2004) Preparation and certification of Re-Os dating reference materials: molybdenites HLP and JDC. Geostand Geoanal Res 28:41–52

Durr SB (1996) Provenance of Xigaze fore-arc basin clastic rocks (Cretaceous, south Tibet). Geol Soc Am Bull 108:669–684

Gaetani M, Garzanti E (1991) Multicyclic history of the northern India continental margin (northwestern Himalaya). AAPG Bull 75:1427–1446

Gao YF, Hou ZQ, Wei RH (2003) Neogene porphyries from Gangdese: petrological, geochemical characteristics and geodynamic significances. Acta Petrol Sinica 19:418–428 (in Chinese with English abstract)

Gao YF, Hou ZQ, Kamber BS, Wei RH, Meng XJ, Zhao RS (2007) Adakite-like porphyries from the southern Tibetan continental collision zones: evidence for slab melt metasomatism. Contrib Mineral Petrol 153:105–120

Gao YF, Yang ZS, Santosh M, Hou ZQ, Wei RH, Tian SH (2010) Adakitic rocks from slab melt-modified mantle sources in the continental collision zone of southern Tibet. Lithos 119:651–663

GGG (2009) Rock sample results at west Guqing area indicate fourth porphyry copper centre at Gangjiang licence area. www.bullabullinggold.com/sites/www.bullabullinggold.com/files/private/West%20Guqing%20Road%20Cut%20Results%2020%20May%202009.pdf

GGG (2008a) Copper oxide recovery at Gangjiang area. www.bullabullinggold.com/sites/www.bullabullinggold.com/files/private/Release_Gangjiang_Cu%20Oxide%20Results%20final.pdf

GGG (2008b) Hole GJ20 at Gelong-East Nading project extends mineralisation further to the west. www.bullabullinggold.com/sites/www.bullabullinggold.com/files/private/Release_Nimu_GJ20%202008-11-11.pdf

Griffin W, Wang X, Jackson S, Pearson N, O'Reilly SY, Xu X, Zhou X (2002) Zircon chemistry and magma mixing, SE China: in-situ analysis of Hf isotopes, Tonglu and Pingtan igneous complexes. Lithos 61:237–269

Griffin W, Pearson N, Belousova E, Saeed A (2006) Comment: Hf-isotope heterogeneity in zircon 91500. Chem Geol 233:358–363

Guo ZF, Wilson M, Liu JQ (2007) Post-collisional adakites in south Tibet: products of partial melting of subduction-modified lower crust. Lithos 96:205–224

Guynn JH, Kapp P, Pullen A, Heizier M, Gehrels G, Ding L (2006) Tibetan basement rocks near Amdo reveal "missing" Mesozoic tectonism along the Bangong suture, central Tibet. Geology 34:505–508

Harris NBW, Xu RH, Lewis CL, Hawkesworth CJ, Zhang YQ (1988) Isotope geochemistry of the 1985 Tibet geotraverse, Lhasa to Golmud. Phil Trans R Soc of London 327:263–285

Harrison TM, Copeland P, Kidd WSF, Yin A (1992) Raising Tibet. Science 255:1663–1670

Hart SR (1984) A large-scale isotope anomaly in the Southern Hemisphere mantle. Nature 309:753–757

Hawkesworth C, Kemp A (2006) Using hafnium and oxygen isotopes in zircons to unravel the record of crustal evolution. Chem Geol 226:144–162

Hou ZQ, Gao YF, Qu XM, Rui ZY, Mo XX (2004) Origin of adakitic intrusives generated during mid-Miocene east–west extension in southern Tibet. Earth Planet Sci Lett 220:139–155

Hou ZQ, Yang ZM, Qu XM, Meng XJ, Li ZQ, Beaudoin G, Rui ZY, Gao YF, Zaw K (2009) The Miocene Gangdese porphyry copper belt generated during post-collisional extension in the Tibetan Orogen. Ore Geol Rev 36:25–51

Hou ZQ, Zheng YC, Yang ZM, Rui ZY, Zhao ZD, Jiang SH, Qu XM, Sun QZ (2012) Contribution of mantle components within juvenile lower-crust to collisional zone porphyry Cu systems in Tibet. Miner Deposita. doi:10.1007/s00126-012-0415-6

Ji WQ, Wu FY, Chung SL, Li JX, Liu CZ (2009) Zircon U-Pb geochronology and Hf isotopic constraints on petrogenesis of the Gangdese batholith, southern Tibet. Chem Geol 262:229–245

Kind R, Ni J, Zhao WJ, Wu JX, Yuan XH, Zhao LS, Sandvol E, Reese C, Nabelek J, Hearn T (1996) Evidence from earthquake data for a partially molten crustal layer in southern Tibet. Science 274:1692–1694

Kinny PD, Maas R (2003) Lu-Hf and Sm-Nd isotope systems in zircon. Rev Mineral Geochem 53:327–341

Leng CB, Zhang XC, Zhou WD (2010) A primary study of the geological characteristics and zircon U-Pb age of the Gangjiang porphyry copper-molybdenum deposit in Nimu. Tibet Earth Science Frontiers 17:185–197 (in Chinese with English abstract)

Li GM, Rui ZY (2004) Petrogenetic and metallogenetic ages for the porphyry copper deposits in the Gangdese metallogenic belt in southern Tibet. Geotecton Metallog 28:165–170 (in Chinese with English abstract)

Li JX, Qin KZ, Li GM, Yang LK (2007) K-Ar and $^{40}Ar/^{39}Ar$ age dating of Nimu porphyry copper orefield in central Gangdese: constrains on magmatic-hydrothermal evolution and metallogenetic tectonic setting. Acta Petrol Sinica 23:953–966

Li JX, Qin KZ, Li GM, Xiao B, Chen L, Zhao JX (2011) Post-collisional ore-bearing adakitic porphyries from Gangdese porphyry copper belt, southern Tibet: melting of thickened juvenile arc lower crust. Lithos 126:265–277

Maheo G, Guillot S, Blichert-Toft J, Rolland Y, Pecher A (2002) A slab breakoff model for the Neogene thermal evolution of South Karakorum and South Tibet. Earth Planet Sci Lett 195:45–58

Mahoney JJ, Frei R, Tejada MLG, Mo XX, Leat PT, Nägler TF (1998) Tracing the Indian Ocean mantle domain through time: isotopic results from old West Indian, East Tethyan, and South Pacific seafloor. J Petrol 39:1285–1306

Marsh TM, Einaudi MT, McWilliams M (1997) 40 Ar/39 Ar geochronology of Cu-Au and Au-Ag mineralization in the Potrerillos District, Chile. Econ Geol 92:784

Martin H (1999) Adakitic magmas: modern analogues of Archaean granitoids. Lithos 46:411–429

Miller C, Schuster R, Klotzli U, Frank W, Purtscheller F (1999) Post-collisional potassic and ultrapotassic magmatism in SW Tibet: geochemical and Sr-Nd-Pb-O isotopic constraints for mantle source characteristics and petrogenesis. J Petrol 40:1399–1424

Mo XX, Hou ZQ, Niu YL, Dong GC, Qu XM, Zhao ZD, Yang ZM (2007) Mantle contributions to crustal thickening during continental collision: evidence from Cenozoic igneous rocks in southern Tibet. Lithos 96:225–242

Mo XX, Niu YL, Dong GC, Zhao ZD, Hou ZQ, Zhou S, Ke S (2008) Contribution of syncollisional felsic magmatism to continental crust growth: a case study of the Paleogene Linzizong volcanic Succession in southern Tibet. Chem Geol 250:49–67

Mo XX, Dong GC, Zhao ZD, Zhu DC, Zhou S, Niu YL (2009) Mantle Input to the Crust in Southern Gangdese, Tibet, during the Cenozoic: zircon Hf isotopic evidence. J Earth Sci-China 20:241–249

Nowell G, Kempton P, Noble S, Fitton J, Saunders A, Mahoney J, Taylor R (1998) High precision Hf isotope measurements of MORB and OIB by thermal ionisation mass spectrometry: insights into the depleted mantle. Chem Geol 149:211–233

Pearce JA, Mei HJ (1988) Volcanic rocks of the 1985 Tibet geotraverse: Lhasa to Golmud. Phil Trans R Soc of London 327:169–201

Qi L, Hu J, Gregoire DC (2000) Determination of trace elements in granites by inductively coupled plasma mass spectrometry. Talanta 51:507–513

Qu XM, Hou ZQ, Li YG (2004) Melt components derived from a subducted slab in late orogenic ore-bearing porphyries in the Gangdese copper belt, southern Tibetan plateau. Lithos 74:131–148

Qu XM, Hou ZQ, Zaw K, Li YG (2007) Characteristics and genesis of Gangdese porphyry copper deposits in the southern Tibetan Plateau: preliminary geochemical and geochronological results. Ore Geol Rev 31:205–223

Qu XM, Hou ZQ, Zaw K, Mo XX, Xu WY, Xin HB (2009) A large-scale copper ore-forming event accompanying rapid uplift of the southern Tibetan Plateau: evidence from zircon SHRIMP U-Pb dating and LA ICP-MS analysis. Ore Geol Rev 36:52–64

Richards JP (2003) Tectono-magmatic precursors for porphyry Cu-(Mo) deposit formation. Econ Geol 98:1515

Richards JP (2009) Postsubduction porphyry Cu-Au and epithermal Au deposit: products of remelting of subduction-modified lithosphere. Geology 37:247–250

Richards JP (2011) High Sr/Y arc magmas and porphyry Cu±Mo±Au deposits: just add water. Econ Geol 106:1075–1081

Rui ZY, Hou ZQ, Qu XM, Zhang LS, Wang LS, Liu YL (2003) Metallogenic epoch of Gangdese porphyry copper belt and uplift of Qinghai-Tibetan Plateau. Mineral Deposit 22:224–232 (in Chinese with English abstract)

Rui ZY, Li GM, Zhang LS, Wang LS (2004) The response of porphyry copper deposits to important geological events in Xizang (Tibet). Earth Sci Front 11:145–152 (in Chinese with English abstract)

Scherer E, Munker C, Mezger K (2001) Calibration of the lutetium-hafnium clock. Science 293:683–687

Schütte P, Chiaradia M, Barra F, Villagómez D, Beate B (2012) Metallogenic features of Miocene porphyry Cu and porphyry-related mineral deposits in Ecuador revealed by Re-Os, $^{40}Ar/^{39}Ar$, and U-Pb geochronology. Miner Deposita 47:383–410

Sillitoe RH (1972) A plate tectonic model for the origin of porphyry copper deposits. Econ Geol 67:184–197

Sillitoe RH (2010) Porphyry copper systems. Econ Geol 105:3–41

Sillitoe RH, Mortensen JK (2010) Longevity of porphyry copper formation at Quellaveco, Peru. Econ Geol 105:1157–1162

Smoliar MI, Walker RJ, Morgan JW (1996) Re-Os ages of group IIA, IIIA, IVA, and IVB iron meteorites. Science 271:1099–1102

Stein HJ, Markey RJ, Morgan JW, Du A, Sun Y (1997) Highly precise and accurate Re-Os ages for molybdenite from the East Qinling molybdenum belt, Shaanxi Province, China. Econ Geol 92:827–835

Sun SS, McDonough WF (1989) Chemical and isotopic systematics of oceanic basalts: implications for mantle composition and processes. In: Saunders AD, Norry MJ (eds) Magmatism in the ocean basins. Geol Soc London Sp Pub 42:313–345

Sun WD, Zhang H, Ling MX, Ding X, Chung SL, Zhou JB, Yang XY, Fan WM (2011) The genetic association of adakites and Cu-Au ore deposits. Int Geol Rev 53:691–703

Turner S, Hawkesworth C, Liu JQ, Rogers N, Kelley S, Vancalsteren P (1993) Timing of Tibetan uplift constrained by analysis of volcanic rocks. Nature 364:50–54

Turner S, Arnaud N, Liu J, Rogers N, Hawkesworth C, Harris N, Kelley S, VanCalsteren P, Deng W (1996) Post-collision, shoshonitic volcanism on the Tibetan plateau: implications for convective thinning of the lithosphere and the source of ocean island basalts. J Petrol 37:45–71

Ulrich T, Günther D, Heinrich CA (2002) The evolution of a porphyry Cu-Au deposit, based on LA-ICP-MS analysis of fluid inclusions: Bajo de la Alumbrera. Argentina: Econ Geol 96:1743–1774

Vervoort JD, Blichert-Toft J (1999) Evolution of the depleted mantle: Hf isotope evidence from juvenile rocks through time. Geochim Cosmochim Acta 63:533–556

Wang XC, Yan ZG, Zhou WD, Jia XK, Li ZH, Wen J, Xu DZ, Yuan JF (2002) Preliminary study on geological features of porphyry type copper deposits in the northwestern Nimu, middle section of Gangdese belt. Tibet Geol and Prospect 38:5–8 (in Chinese with English abstract)

Wen DR, Chung SL, Song B, Iizuka Y, Yang HJ, Ji JQ, Liu DY, Gallet S (2008) Late Cretaceous Gangdese intrusions of adakitic geochemical characteristics, SE Tibet: petrogenesis and tectonic implications. Lithos 105:1–11

Williams H, Turner S, Kelley S, Harris N (2001) Age and composition of dikes in Southern Tibet: new constraints on the timing of east–west extension and its relationship to postcollisional volcanism. Geology 29:339–343

Williams HM, Turner SP, Pearce JA, Kelley SP, Harris NBW (2004) Nature of the source regions for post-collisional, potassic magmatism in southern and northern Tibet from geochemical variations and inverse trace element modelling. J Petrol 45:555–607

Woodhead JD, Hergt JM (2005) A preliminary appraisal of seven natural zircon reference materials for in situ Hf isotope determination. Geostand Geoanal Res 29:183–195

Woodhead J, Hergt J, Davidson J, Eggins S (2001) Hafnium isotope evidence for 'conservative' element mobility during subduction zone processes. Earth Planet Sci Lett 192:331–346

Wu FY, Yang YH, Xie LW, Yang JH, Xu P (2006) Hf isotopic compositions of the standard zircons and baddeleyites used in U-Pb geochronology. Chem Geol 234:105–126

Yang JH, Wu FY, Wilde SA, Xie LW, Yang YH, Liu XM (2007) Tracing magma mixing in granite genesis: in situ U-Pb dating and Hf-isotope analysis of zircons. Contrib Mineral Petrol 153:177–190

Yang ZS, Hou ZQ, Meng XJ, Liu YC, Fei HC, Tian SH, Li ZQ, Gao W (2009) Post-collisional Sb and Au mineralization related to the South Tibetan detachment system, Himalayan orogen. Ore Geol Rev 36:194–212

Yin A, Harrison TM (2000) Geologic evolution of the Himalayan-Tibetan Orogen. Annual Rev Earth Planet Sci 28:211–280

Yin A, Harrison TM, Ryerson FJ, Chen WJ, Kidd WSF, Copeland P (1994) Tertiary structural evolution of the Gangdese thrust system, southeastern Tibet. J Geophys Res 99:18175–18201

Zhang LC, Xiao WJ, Qin KZ, Zhang Q (2006) The adakite connection of the Tuwu-Yandong copper porphyry belt, eastern Tianshan, NW China: trace element and Sr-Nd-Pb isotope geochemistry. Miner Deposita 41:188–200

Zheng YY, Gao SB, Cheng LJ, Li GL, Feng NP, Fan ZH, Zhang HP, Guo JC, Zhang GY (2004) Finding and significances of Chongjiang porphyry copper (molybdenum, aurum) deposit. Tibet Earth Sci-J of China Univ of Geosci 29:333–339 (in Chinese with English abstract)

Zhou WD, Zhang QS (2010) A preliminary study of geological features for the Nimu Gangjiang porphyry Cu-Mo deposit. Acta Geol Sichuan 30:416–419 (in Chinese with English abstract)

Zhu DC, Pan GT, Chung SL, Liao ZL, Wang LQ, Li GM (2008) SHRIMP zircon age and geochemical constraints on the origin of Lower Jurassic volcanic rocks from the Yeba Formation, Southern Gangdese, South Tibet. Int Geol Rev 50:442–471

Zinder A, Hart SR (1986) Chemical geodynamics. Annu Rev Earth Pl Sci 14:493–571